Astron. Astrophys. 362, 683–690 (2000)

ASTRONOMY AND ASTROPHYSICS

Chromospheric two-component NLTE modelling of the binary system V 711 Tau = HR 1099

A.C. Lanzafame[1], **I. Busà**[1], **and M. Rodonò**[1,2]

[1] Dipartimento di Fisica e Astronomia, Università di Catania, Viale Andrea Doria 6, 95125 Catania, Italy
[2] Osservatorio Astrofisico di Catania, Viale Andrea Doria 6, 95125 Catania, Italy

Received 2 March 2000 / Accepted 8 May 2000

Abstract. In this paper we present the first two-component, semi-empirical chromospheric model of the RS CVn binary system V 711 Tau based on detailed fits of Hα and Mg II h line profiles.

Synthetic Hα and Mg II h line profiles are computed by means of NLTE radiative transfer calculations. Using the observed Emission Measure distribution to constrain the transition region structure and the photospheric *Next-Generation* model with $\log(g)$=3.5 and $T_{\rm eff}$ =4800 K, we have built a grid of chromospheric models for the K1 IV component of the binary system by means of spline interpolations between photospheric and transition region models. With such interpolations the free parameters are restricted to the temperature minimum and the position of an interpolation knot. We find that a mean single-component model cannot satisfactorily reproduce the observed line profiles. Chromospheric Doppler Imaging is then used to consider the chromospheric emission as due to two different components of known surface coverage and emission. Extensive grids of semi-empirical chromospheric models are built separately for the two components and the weighted-combined synthetic Hα and Mg II h profiles are compared with observations. Two-component synthetic line profiles reproduce the observed Hα and Mg II h in detail, indicating that the *broad* and *narrow* components can be interpreted in terms of radiative transfer effects in different atmospheric structures for the active and quiet regions. From this analysis we infer information on physical properties of the active region, from which the *broad* component originates, with respect to the remaining chromosphere from which the *narrow* component originates. We show also that the variability outside flares can be reproduced considering slightly different models for the active region.

Key words: stars: activity – stars: atmospheres – line: formation – stars: binaries: spectroscopic – stars: imaging – stars: individual: HR 1099

1. Introduction

The process leading to the heating of the upper layers of solar and stellar atmospheres is closely related to the presence of magnetic fields. The way in which the energy generated in the convection zone is transported and dissipated throughout the stellar chromosphere, transition region and corona remains, however, poorly understood.

The binary system V 711 Tau, being one of the most active RS CVn spectroscopic binary systems ($P_{\rm rot} \approx 2^d.8$) with a G5-type component of luminosity class V and a cooler K1 IV component, is well suited for the study of chromospheric heating in late type stars. Its tidally induced rapid rotation, combined with the deepened convection zone of a post-main sequence envelope, is responsible of maximal chromospheric activity for its spectral class. The primary, more massive component of the close binary (the K star) shows, infact, very strong and variable Ca II H & K, Hα and UV emission that are indicative of high chromospheric activity (Rodonò et al. 1987; Neff et al. 1995; Dempsey et al. 1996; Robinson et al. 1996). V 711 Tau has been observed at radio (Owen et al. 1976; Trigilio et al. 1993; Umana et al. 1995), soft X ray (Agrawal & Vaidya 1988), and EUV wavelengths (Drake et al. 1994).

UV observations from IUE and GHRS have established the presence of broad wings in spectral lines of active stars (V 711 Tau, AU Mic, and Capella) as opposed to those of less active stars (like Procyon), which do not show evidence of such broad component. Wood et al. (1996) found that transition region lines in V 711 Tau have broad wings associated to the K star, which are even more prominent than in AU Mic and Capella. They interpreted such broad component as due to microflaring. Dempsey et al. (1996) and Wood et al. (1996) revealed broad wings in the chromospheric Mg II h and k lines of V 711 Tau too, and suggested that the broad component phenomenon might extend into the chromosphere. Montes et al. (1997) revealed broad and variable wings on the Hα chromospheric line of the K star of V 711 Tau. These authors found evidence of a close correlation between the broad component contribution to the total emission and the degree of stellar activity by comparing 25 binary systems characterised by a wide range of activity level. Such a correlation was confirmed by Wood et al. (1997).

Busà et al. (1999), using V 711 Tau IUE data with an extensive coverage of more than two complete orbits, detected rotational modulation of the broad component of the chromospheric Mg II h line profiles. By a Doppler Imaging Technique (DIT) study of an extensive set of spectra unaffected by flar-

Send offprint requests to: A.C. Lanzafame
Correspondence to: acl@sunct.ct.astro.it

ing, they took advantage from the extensive phase-coverage to get a tight constraint on the quasi-constant narrow component flux and, consequently, on the flux attributed to the broad, more variable component, with its centroid correlated with rotation. These authors suggested that the phase-limited GHRS data sets did not allow to detect rotational modulation, which was found from the extensive phase coverage of the IUE data. The same authors found that the broad component may be attributed to a localised area at high latitude ($> 67°$) on the K star surface. This is consistent with the stable photospheric spot configuration observed from 1981 to 1992 on V 711 Tau (Dorren & Guinan 1982, Rodonò et al. 1986, Vogt et al. 1999) and with the strong magnetic field ($\approx$ 1000 G) detected by Zeeman Doppler Imaging (Donati et al. 1990; 1992) and localised at high latitudes on the K star over about 18% of the stellar surface.

A widely adopted method to get information on physical properties of chromospheric layers of active stars is the NLTE radiative transfer semi-empirical modelling (see, e.g., Vernazza et al. 1981; Fontenla et al. 1993; Lanzafame 1995; Mauas et al. 1997). Late-type stars with Hα in emission show a fairly stable chromospheric emission outside flares (see. e.g., Byrne et al. 1998). This reinforces the hypothesis that chromospheres are globally in a quasi-stationary state, modulated mainly by the stellar activity cycle, in which the temperature-density structure results from the balance between global dissipation of non-radiative energy and radiative cooling (see Kalkofen et al. 1999). Furthermore, the application of NLTE semi-empirical chromospheric modelling to such stars can effectively be based on optical observations. This is because lines such as the Hα become dominated by electron-collision excitation processes, which make them effective chromospheric diagnostics (see also Cram & Mullan 1979; Cram & Giampapa 1987; Houdebine & Panagi 1990).

In this paper we have used the diagnostic power of Hα and Mg II h lines to explore the nature of the *broad* and *narrow* components detected in the chromospheric emission of V 711 Tau. We present an extensive semi-empirical modelling of Hα and Mg II h lines based on NLTE radiative transfer calculations. Use is made of the transition region emission measure to constrain the upper chromospheric structure of the models. Furthermore, on the base of the Busà et al. (1999) results, we have built a grid of two-component semi-empirical models that gives the possibility of verifying whether the chromosphere of the K star is characterised by two different plasma regimes or if a single model can satisfactorily represent the mean chromosphere. This model refinement allows both to check the validity of Doppler Imaging results as well as to get physical information on active and "quiet" region structures.

2. Observations

Hα observations where obtained in September 1997 at the *M. G. Fracastoro* observing station of Catania Astrophysical Observatory with the 91-cm Cassegrain telescope equipped with the REOSC echelle spectrograph in high dispersion mode (Catalano, S., Frasca, A., Marino, G., Marilli, E., 1999, private communication). The spectra were taken with typical exposure times of 20–25 min and signal-to-noise ratio (S/N) $\sim$100 in the continuum close to Hα, and were recorded on a 1150x800 pixels EEV 05–20 CCD with a spectral resolution of about 0.47 Å in the Hα region.

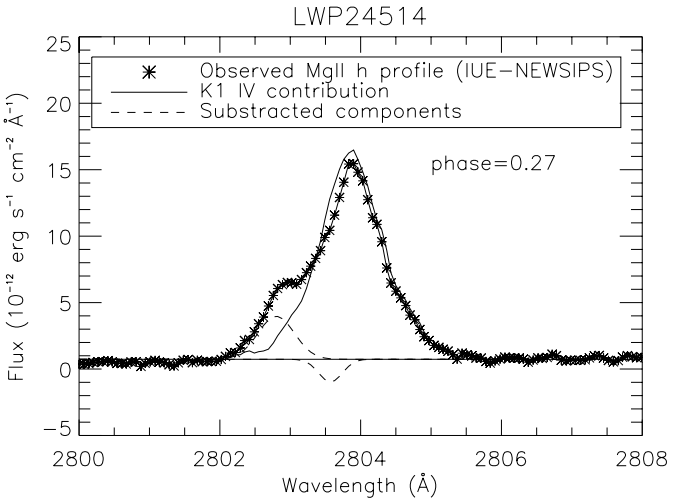

Fig. 1. IUE LWP 24514 Mg II h line profile of V 711 Tau. The K1 IV spectrum (solid line) is obtained by subtracting the G5 V contribution and the ISM absorption (dashed lines), as in Busà et al. (1999).

Mg II h observations of V 711 Tau were obtained by the IUE satellite in December 1992 during a Multi-Site Continuous Spectroscopy (MUSICOS) campaign (Huang et al. 1995). Spectral resolution was about 0.2 Å in the Mg II region. The analysis presented in this paper is focused on the NEWSIPS (New Spectral Image Processing System) spectrum LWP24514. This is taken close to quadrature (phase=0.27), and it is not apparently affected by flares or scattered light (for details, see Busà et al. 1999).

Orbital phases were computed using the ephemeris HJD 2,442,766.080 + 2.83774E (Strassmeier et al. 1993), with an accuracy $\Delta\phi = 0.01$.

The K1 IV Mg II h profile (Fig. 1) has been obtained by subtracting the G5 V spectrum and the ISM absorption, as in Busà et al. (1999).

The relative flux has been obtained by normalising with respect to the continuum emission estimated over a large spectral range around the Mg II h and k, as shown in Fig. 2.

3. Computational method

3.1. Modelling the photosphere

For the photospheric part of the K1 IV model atmosphere we have adopted the *Next-Generation* (N-G) model (Hauschildt, P.H., 1999, private communication) with effective temperature $T_{\rm eff} = 4800$ K, surface gravity $\log(g) = 3.5$, metal abundance $[\frac{A}{H}] = 0.0$, and microturbulence $\xi = 2.0$ km s^{-1}. The $T_{\rm eff}$ adopted is 50 K hotter than estimated for the K-type star (Vogt & Penrod, 1983) and $\log(g)$ is at the upper limit of the range found by Fekel (1983) from estimates of stellar radius and or-

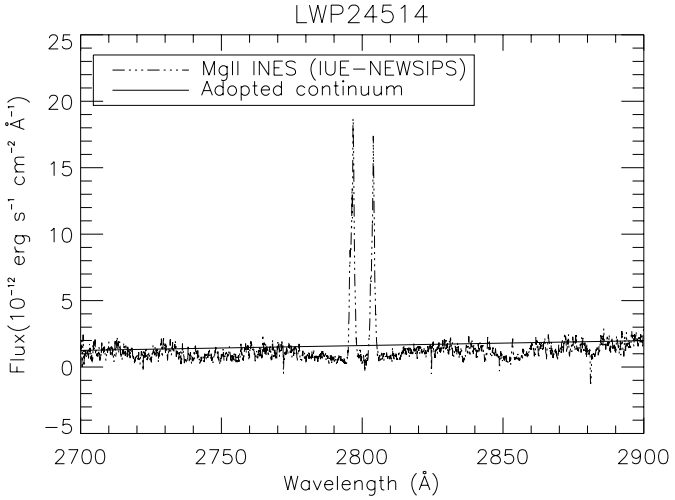

Fig. 2. IUE LWP 24514 spectrum in the wavelength range including the Mg II lines and the estimated continuum emission that was adopted to normalise the Mg II h profile shown in Fig. 1.

bital inclination $\hat{\imath}$. However, the estimated $T_{\rm eff}$ for the K star is probably uncertain by $\pm\,100$ K. The NLTE radiative transfer calculation gives, for the photospheric model adopted, a continuum flux $F^K_{\rm cont}$(at Hα)=3.3·10^6 erg cm^{-2} s^{-1} Å^{-1}, which is in satisfactory agreement with the observational value $F^K_{\rm cont}$(at Hα)$\approx 3.1\cdot10^6$ erg cm^{-2} s^{-1} Å^{-1} obtained by Frasca & Catalano (1994) using the Barnes and Evans relation.

For the G5 V model we have adopted the photospheric N-G model with $T_{\rm eff}$=5400 K, $\log(g)$=4.0, $[\frac{A}{H}] = 0.0$ and $\xi = 2.0$ km s^{-1}. The measured $T_{\rm eff}$and $\log(g)$ for the G-type star are, respectively, 5450 K and 4.27. The adopted effective temperature is therefore close to the observational estimate and probably within errors. On the other hand, the observed $\log(g)$ is in between two LTE models of the N-G grid, at $\log(g) = 4.0$ and $\log(g) = 4.5$. A comparison of the resulting synthetic spectra with the observations between 6600 and 6700 Å leads to the selection of the model with $\log(g) = 4.0$.

3.2. Modelling the transition region

Models for the lower transition region (TR) are obtained by combining the temperature gradient as a function of the emission measure averaged over $\Delta\log(T_{\rm e}) = 0.30$ ($EM_{0.3}$ - see, e.g., Griffith & Jordan 1998) and the pressure variation from the equation of hydrostatic equilibrium (see, e.g., Harper 1992). This gives the relationship

$$P^2_{\rm T}(T_2) - P^2_{\rm T}(T_1) = 2(1.4)^2 m_{\rm p} g k \times \int_{T_1}^{T_2} [EM_{0.3}(1+1.1x) + \tfrac{1.4 x m_{\rm p}\xi^2 EM_{0.3}}{2kT}]dT \quad (1)$$

where $m_{\rm p}$ is the H^+ mass, k is the Boltzmann constant and $x \equiv N_{\rm H}/N_{\rm e}$. The latter equation, together with an estimate of the total pressure in a layer, allows one to find the pressure as a function of temperature for the TR model. The total particle density ($N_{\rm tot}$), gas pressure ($P_{\rm G}$), microturbulence pressure ($P_{\rm turb}$) and electron density ($N_{\rm e}$) are then obtained according to the following relations

$$\begin{aligned} N_{\rm tot} &= P_{\rm T}/(k\,T + \tfrac{1}{2} m_{\rm p}\,\mu\,\xi^2) \\ P_{\rm G} &= N_{\rm tot}\,k\,T \\ P_{\rm turb} &= \tfrac{1}{2} N_{\rm tot}\,m_{\rm p}\,\mu\,\xi^2 \\ N_{\rm e} &= N_{\rm tot}/(1.+1.1\,x) \end{aligned} \quad (2)$$

The emission measure and the electron density have been derived from Griffiths & Jordan (1998), who obtained the Volumetric Emission Measure (VEM) and $N_{\rm e} = 5.0\cdot10^{11}$ cm^{-3} at $\log(T) = 4.7$. Microturbulence is included adopting the relationship $\xi(T) = \xi(T_0)\cdot(T/T_0)^{1/4}$ given by Jordan (1991) and ξ=97 km s^{-1} at $\log(T) = 4.7$, as estimated by Griffiths & Jordan (1998).

The evaluation of $x = N_{\rm H}/N_{\rm e}$ is based on an iterative procedure. From an initial estimate of $x(T)$ the TR model is computed, than the NLTE radiative transfer equations are solved to give a new evaluation of $x(T)$ and the procedure is iterated until convergence is reached. In Table 1 we list the VEM, ξ, and $N_{\rm H}/N_{\rm e}$ as function of temperature, used to calculate the TR model.

Single-component models for the low transition region of the mean K star's surface have been built under the assumption that the total observed VEM arises uniformly from the K star. In this case, the Emission Measure is given by $EM_{0.3} \approx VEM/4\,\pi\,R^2_{K1}$ (see Table 1, third column). The electron density is $N_{\rm e} = 5.0\cdot10^{11}$ cm^{-3} at $\log(T) = 4.7$ as estimated by Griffiths & Jordan (1998).

Two-component TR models are further refinements in which the Busà et al. (1999) chromospheric Doppler Imaging is used to identify two different components of known surface coverage and emission. The total VEM is assumed to be the sum of three

Table 1. Measured VEM for V 711 Tau (from GHRS Data, by Griffiths & Jordan 1998). Emission Measure for the mean K1 IV star, the broad and narrow components, microturbulence velocity and $N_{\rm H}/N_{\rm e}$ adopted for the lower TR models.

		Mean	Narrow	Broad		
$\log(T)$	$\log(VEM)$	$\log(EM_{0.3})$			ξ	$N_{\rm H}/N_{\rm e}$
K	cm^{-3}	cm^{-5}			km s^{-1}	
5.3	51.88	27.91	27.81	28.19	137	0.81
5.2	51.97	28.00	27.90	28.28	117	0.81
5.1	52.15	28.18	28.08	28.46	100	0.81
5.0	52.30	28.33	28.23	28.61	87	0.81
4.9	52.42	28.45	28.35	28.73	80	0.81
4.8	52.45	28.48	28.38	28.76	67	0.81
4.7	52.60	28.63	28.53	28.91	60	0.81
4.6	52.73	28.76	28.66	29.04	54	0.81
4.5	52.80	28.83	28.73	29.11	52	0.81
4.4	52.95	28.98	28.88	29.26	47	0.91
4.3	53.10	29.13	29.03	29.41	40	0.95
4.2	53.40	29.43	29.33	29.71	33	1.18
4.1	54.12	30.15	30.05	30.43	17	1.96
4.0	55.05	31.08	30.98	31.36	13.	3.31

Table 2. Chromospheric DIT results on V 711 Tau from Busà et al. (1999). The filling factor $(R/R_{\rm K1})^2$ is estimated assuming a plage coverage equal to that of a polar cap extending northern than the DIT estimated latitude ($> 67^\circ$). f is the Mg II h flux at Earth.

	G5 V	K1 IV Broad	K1 IV Narrow
$(R/R_{\rm K1})^2$	0.11	0.15	0.85
$f/f_{\rm tot}$	0.050	0.285	0.665

components, formed in the G and K star TR, the latter giving rise to a broad and a narrow emission component, i.e.:

$$VEM_{\rm tot} = VEM_{\rm G} + VEM_{\rm br} + VEM_{\rm na} \quad (3)$$

From Table 2, $VEM_{\rm G5} \approx 5\% VEM_{\rm tot}$, $VEM_{\rm K1} \approx 95\% VEM_{\rm tot}$ of which $VEM_{\rm br} \approx 30\% VEM_{\rm K1}$ and $VEM_{\rm na} \approx 70\% VEM_{\rm K1}$. The emission measure of each component is given by $EM_{0.3}(\rm comp) \approx VEM/4\,\pi\,R^2_{\rm comp}$ (Table 1, fourth and fifth columns).

The electron density in the quiet and active components is estimated considering the proportionality of the emitted radiative power $\wp$ (erg s^{-1}) to the electron density squared and to the emitting area in the optically thin regime. From Table 2 we obtain $\wp_{\rm na} \approx 0.7\,\wp_{\rm K1}$ and $\wp_{\rm br} \approx 0.3\,\wp_{\rm K1}$. Therefore, from the mean electron density ($\overline{N_{\rm e}} = 5.0 \cdot 10^{11}$ cm^{-3} at $\log(T) = 4.7$), we estimate

$$\begin{aligned} N_{\rm e}(\log(T_{\rm e}) = 4.7)_{\rm na} &= \overline{N_{\rm e}} \sqrt{\tfrac{0.7}{0.85}} = 4.5 \cdot 10^{11}\ {\rm cm}^{-3} \\ N_{\rm e}(\log(T_{\rm e}) = 4.7)_{\rm br} &= \overline{N_{\rm e}} \sqrt{\tfrac{0.3}{0.15}} = 7.1 \cdot 10^{11}\ {\rm cm}^{-3} \end{aligned} \quad (4)$$

The distribution of turbulent velocity has been assumed the same for the narrow and broad components and, as in the single-component modelling, it has been calculated according the relationship given by Jordan (1991) and the estimate of Griffiths & Jordan (1998) at $\log(T) = 4.7$.

3.3. Chromospheric models

To complete the model atmospheres, chromospheric models are generated by a smooth interpolation (using a spline) between the photosphere and the transition region. In such interpolation, a grid of temperature minima are considered as starting points for the chromospheric rise. Between the temperature minimum and the base of the transition region, a grid of 5×5 interpolation knots determines the behaviour of the chromospheric structures, on which we impose a monotonic temperature dependence on column mass ($dT/dm \leq 0$). We consider a grid of nine values of $T_{\rm min}$ in the range between ∼3300 K and 4700 K with a step of less than 200 K. In this way we generate more than one hundred mean, one hundred broad and one hundred narrow atmospheric models.

Table 3. Energy levels included in the H model atom.

	Ion	level	E (cm^{-1})	2J+1
1	H I	n=1	0.000	2
2	H I	n=2	82259.047	8
3	H I	n=3	97492.281	18
4	H I	n=4	102823.883	32
5	H I	n=5	105291.648	50
6	H II	n=∞	109678.766	1

Table 4. Energy levels included in the Mg model atom.

	Ion	level	E (cm^{-1})	2J+1
1	Mg I	$2p^6 3s3s\ ^1S$	0.000	1
2	Mg I	$2p^6 3s3p\ ^3P^O$	21890.303	9
3	Mg I	$2p^6 3s3p\ ^1P^O$	35050.383	3
4	Mg II	$2p^6 3s\ ^2S_{1/2}$	61671.050	2
5	Mg II	$2p^6 4p\ ^2P^O_{1/2}$	97340.360	2
6	Mg II	$2p^6 4p\ ^2P^O_{3/2}$	97431.930	4
7	Mg II	$2p^6 4s\ ^2S_{1/2}$	131476.000	2
8	Mg II	$2p^6 3d\ ^2D_{5/2}$	133161.240	6
9	Mg II	$2p^6 3d\ ^2D_{3/2}$	133162.110	4
10	Mg III	$2p^6\ ^1S^O$	182938.690	1

3.4. Atomic models

We have used version 2.2 of the code MULTI (Carlsson 1986) to solve the combined radiative transfer and statistical equilibrium equations for the H atomic model shown in Table 3 and for the Mg atomic model of Table 4. The electron density is calculated, in the H run, iterating the NLTE solution and the equation of hydrostatic equilibrium to convergence. The electron density produced by the H calculation is then used to solve the Mg radiative transfer and statistical equilibrium equations. The population densities obtained from the H calculation are used to obtain the background NLTE source function in the Mg calculation.

The whole grid of atmospheric models have been considered in the radiative transfer calculation for H and Mg. For a comparison with the observations, we have selected those models that converge to solution both for H and Mg.

4. Results

4.1. Single-component models

We first attempted to fit Hα and Mg II h using a single-component model to describe the whole chromosphere of the K star. Fig. 3 shows the grid of single-component models for the K star that have been compared with the observed spectra. Six temperature minima of the initial nine-elements grid give atmospheric models with $dT/dm \leq 0$ and converge to solution for both H and Mg.

The synthetic Hα line profile is obtained as the sum of synthetic lines from the G star model and the K star single-component model. The Mg II h line is obtained as the sum of the continuum emission obtained from the G model and the

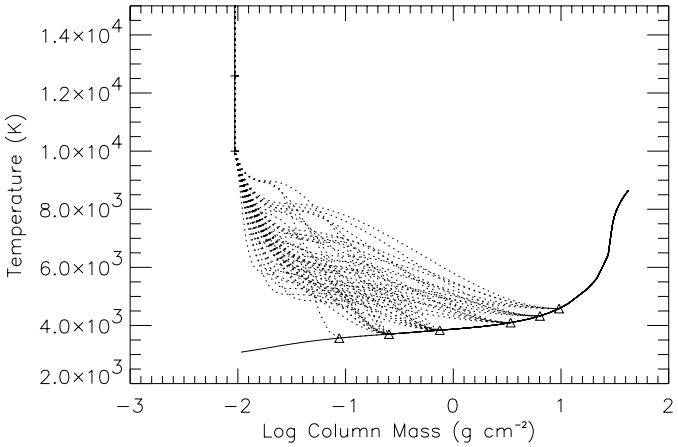

Fig. 3. Grid of selected single-component models for a comparison with the observations. The models are generated by a spline interpolation (dotted lines) between the photospheric and the transition region models (solid lines), selecting those models with $dT/dm \leq 0$ and which converge to solution for both H and Mg. Triangles indicate the temperature minima considered as the starting points for the chromospheric rise.

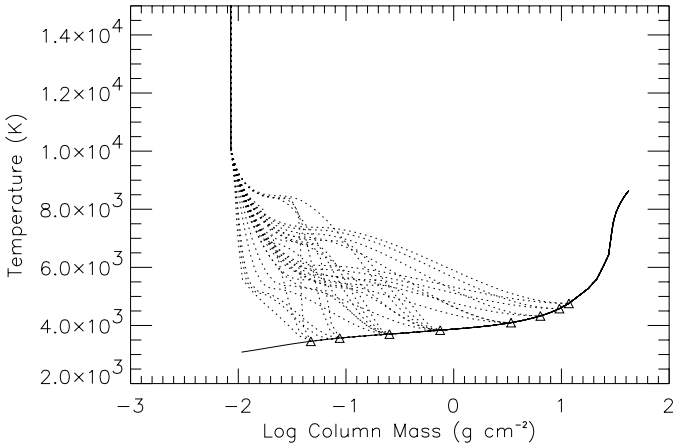

Fig. 4. Grid of narrow-component models selected for comparison with observations (see Fig. 3 for details).

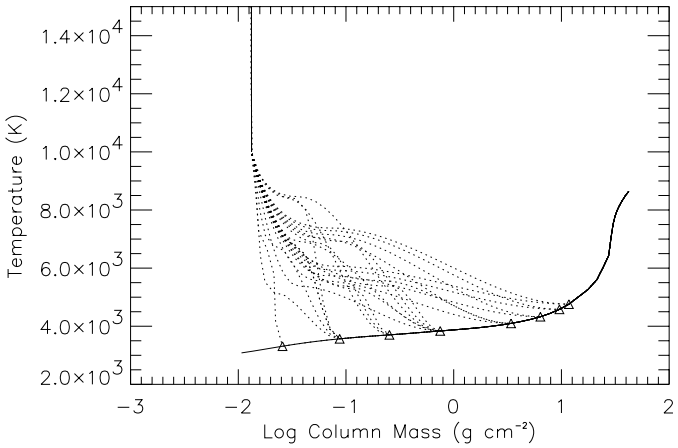

Fig. 5. Grid of broad-component models selected for comparison with observations (see Fig. 3 for details).

Mg II h from the K single-component model. The Mg II h line produced by the G star is not taken into account since it is removed from the observations before comparison with synthetic spectra. Convolution for rotational and instrumental profile, as well as normalisation and wavelength shifts to account for orbital velocities, are applied to synthetic spectra.

Single-component models produce lines that are either too high at central peak or too broad. However, from this preliminary exercise we derive the qualitative dependence of the profiles from the chromospheric structure. Continuum emission in the Hα region is found to be strongly dependent on both the position of the interpolation knot (column mass and temperature), which mimics the position of a chromospheric plateau, and the temperature minimum. The continuum close to Hα is in good agreement with the observations of Frasca & Catalano (1994) only for the lowest temperature minimum and the lowest chromospheric temperature in our grid of models. Mg II h and Hα FWHMs are mainly dependent on chromospheric temperature, being larger for higher temperatures. When a high chromospheric temperature is considered, EW's strongly depend on the temperature minimum via the temperature gradient induced on the lower chromosphere, decreasing with increasing temperature minimum.

It is interesting to note that each model produce unique line profiles. Therefore, when line profiles are compared with observations and the constraints described above are adopted, the method does not suffer of non-uniqueness problems.

4.2. Two-component models

Figs. 4 and 5 show the grids of narrow- and broad-component models which have been considered in modelling the Hα and Mg II h line profiles.

The resulting two-component profiles for Hα and Mg II h are obtained by combining narrow and broad profiles. The G star contribution is included as before.

The synthetic profile obtained from each narrow model is convolved with the rotational profile of the K star (38 km s^{-1}), then shifted according to the radial velocity of the K star at the observed phase. The synthetic profile from the broad model is convolved with the rotational profile for the active region at latitude $\approx$ 67° (14 km s^{-1}) and shifted with respect to the narrow-component according to the radial velocity dependence on rotational phase found by Busà et al. (1999). The broad and narrow component profiles are then weighed according their $(d/R_{\rm comp})^2$ factor, summed together, convolved with the intrumental profile and normalised prior to comparison with observations.

Comparison with observations shows that two-component models overcome the limitations of single-component models, giving satisfactory fits of Hα and Mg II h profiles, as well as of the continuum close to Hα.

Broad models are characterised by a stronger continuum emission in the Hα region. Nevertheless, because of the small

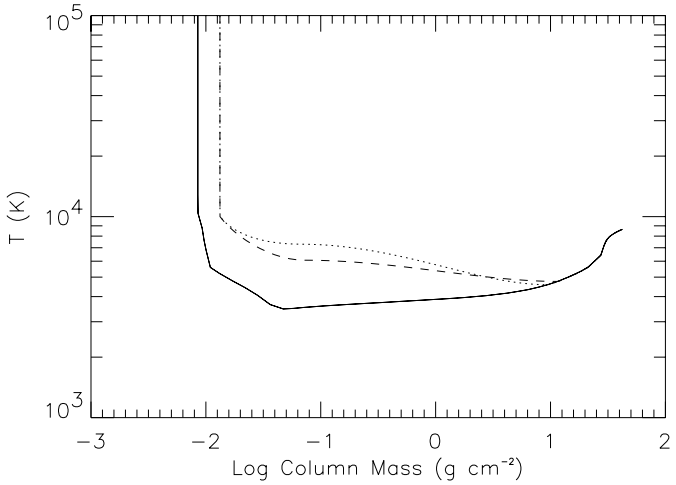

Fig. 6. Narrow model (a) (solid line) selected as the one that best reproduces the continuum emission in the Hα region. Broad model (A) (dotted line) selected as the one which, combined with the (a) model, best reproduces both the observed Hα profile and continuum, and broad model (C) selected as the one which, combined with the (a) model, best reproduces both the observed Mg II h profile and continuum.

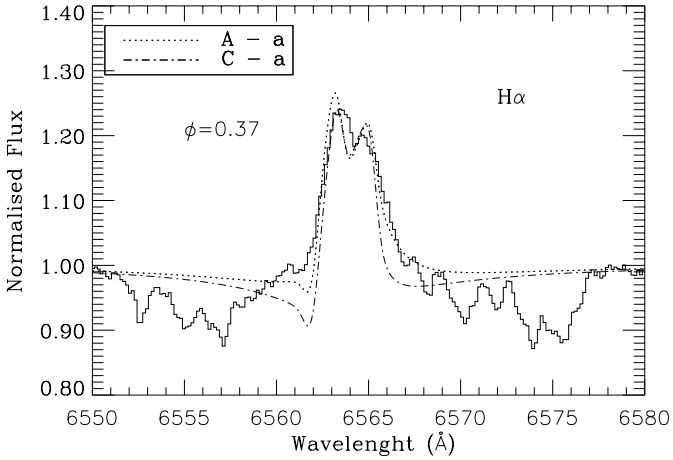

Fig. 7. Synthetic Hα line profiles calculated combining the narrow (a) with the broad (A) (dotted line) and (C) models (dashed line) compared with the observed Hα profile. This is best reproduced using the A-a two components' model.

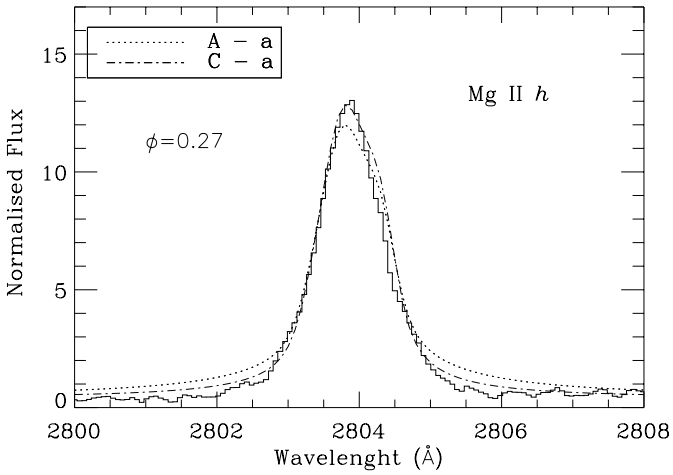

Fig. 8. Synthetic Mg II h line profiles calculated combining the narrow (a) with the broad (A) (dotted line) and (C) models (dashed line) compared with the observed Mg II h profile. This is best reproduced using the C-a two components' model.

filling factor of the active region, the two-component continuum flux at Earth is dominated (for more than 65% of the total contribution) by the narrow-component (which describes the quiescent background of the K star).

We have selected as the best narrow model for the quiet K chromosphere the one that best repoduces the continuum emission in the Hα region. This narrow model is indicated with (a) in Fig. 6. The continuum emission in the Hα region obtained from the (a) model is about $3.2{\cdot}10^6$ erg cm^{-2} s^{-1}, in good agreement with the value $3.1{\cdot}10^6$ erg cm^{-2} s^{-1} estimated by Frasca & Catalano (1994). Then, we have selected broad models which, combined with the (a) model, best reproduce both line profiles and continuum. Since comparison is made with observations at different epochs (1992 for Mg II h and 1997 for Hα), we have selected broad models that either closely reproduce the observed Hα and gives the Mg II h within the estimated variability, or viceversa. The selected broad models are indicated with (A) and (C) in Fig. 6. The observed Mg II h profile is best reproduced using the (C) broad model, while the observed Hα profile is best reproduced using the (A) model (see Figs. 7 and 8). Both models, however, appear to be satisfactorily compatible with the observations.

Fig. 6 shows that the broad (A) and (C) models, which describe the structure of the K star active region at two different epochs. Both (A) and (C) have chromospheric temperature, temperature minimum and transition region pressure much higher than the narrow (a) model, which describe the stellar chromosphere outside the active region.

The a-C model gives Hα wings that are somewhat narrower than the observed profile, while the a-A model gives Mg II h wings that are somewhat broader than the observed profile. This could indicate that the broad (A) model describes the polar active region of the K star in an higher activity regime than the broad (C), and reinforces the idea that, for V 711 Tau and similar objects, the main chromospheric variability outside of flares is due to a gradual evolution of active regions (see, e.g., Byrne et al. 1998).

Figs. 9 and 10 show the Hα and Mg II h line computed from the narrow (a) and broad (A) or (C) models, respectively. Here, no convolution for rotational and instrumental profiles, nor weighting for the d^2/R^2 factor, nor normalisation or shifts have been applied. The profiles are characterised by a strong central reversal, that is much less evident in the final profiles (see Figs. 7 and 8) because convolutions and shifts have been applied to the narrow and broad profiles. The broad models show much stronger emission both in the lines and in the continuum with respect to the narrow model. Furthermore, the profiles obtained from the broad models have larger FWHM with respect to the profiles obtained from the narrow (a), despite the ξ distri-

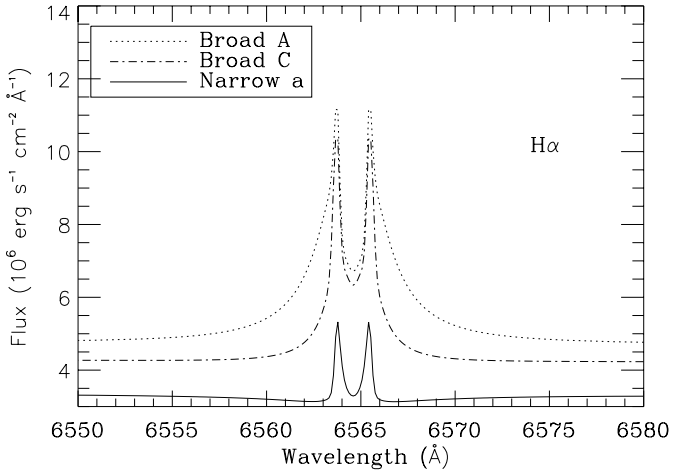

Fig. 9. Hα line flux at the star, from the narrow (a) (solid line), the broad (A) (dotted line) and (C) (dashed line) models. No convolution, shifts, weighting for the d^2/R^2 factor, nor normalisation have been applied.

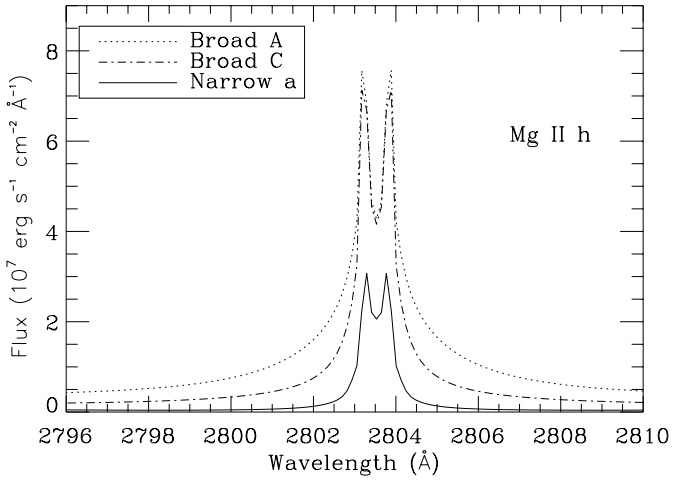

Fig. 10. Mg II h line flux at the star, from the narrow (a) (solid line), the broad (A) (dotted line) and (C) (dashed line) models. No convolution, shifts, weighting for the d^2/R^2 factor, nor normalisation have been applied.

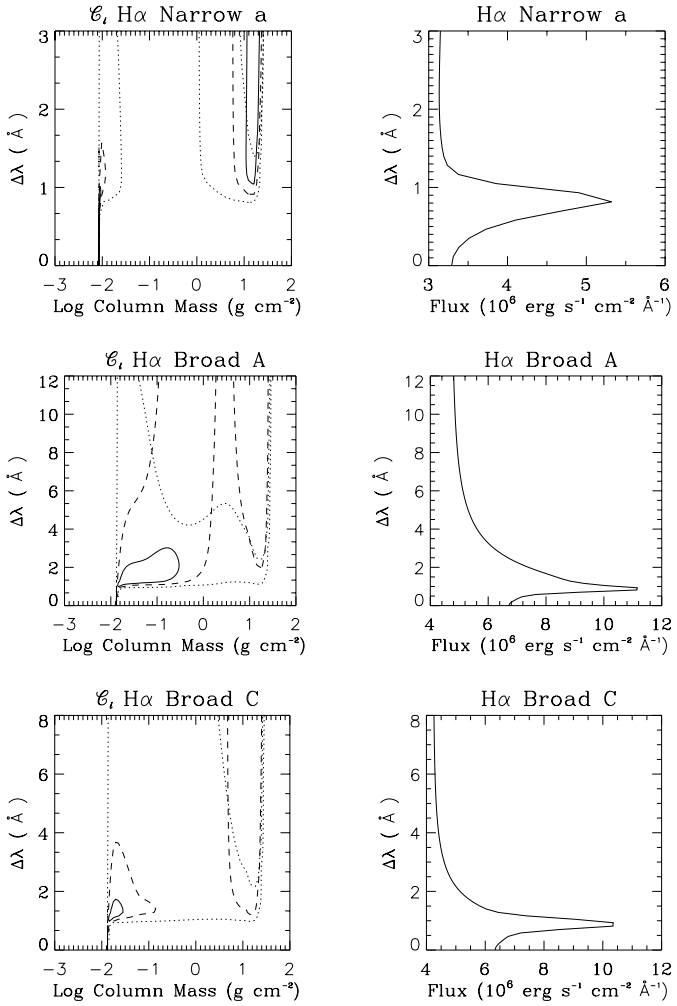

Fig. 11. Contribution function to the emergent radiation ($\mathcal{C}_l$) for the Hα line obtained from the narrow (a), broad (A), and broad (C) models (left panels) and emergent line flux (right panels). The maximum of the contribution function is set equal to one. The contour plot indicates the fractions 0.6 (solid), 0.2 (dashed) 0.05 (dotted).

bution is assumed the same for all models. The profiles obtained from the broad models (A) and (C) show very similar cores but different wings.

Line contribution functions to the emergent radiation ($\mathcal{C}_l$ - see Achmad et al. 1991 for the definition adopted) indicate that the core of both Hα and Mg II h originates from the base of the TR ($\log(m) \approx -2$) for both narrow (a), and broad (A) or (C) models (Figs. 11 and 12). The similarity in the emission core of the lines from the broad (A) and (C) models is the result of having fixed the lower TR pressure. The narrow (a) model produces a weaker emission core because of its lower TR pressure.

Hα wings form mainly at the base of the TR for model narrow (a), in the whole chromospheric layers for broad (A), and mainly in the upper chromospheric layers for broad (C). Mg II h wings form mainly in the upper chromospheric layers for models narrow (a), broad (A), and broad (C). The difference in wings width from models (A) and (C) is mainly due to the different extension of the chromospheric region in which the wings are formed. While the continuum emission close to Hα arises only from layers below the temperature minimum in model narrow (a), broad models produce a chromospheric contribution to the continuum emission.

5. Conclusions

From extensive NLTE radiative transfer semi-empirical modelling, we conclude that the broad component observed in the chromospheric lines of V 711 Tau is due to a localised area on the K1 IV star. Our analysis indicates that the inhomogeneity on the K1 IV star chromosphere found by Doppler Imaging (Busà et al. 1999) corresponds to a different plasma regime with respect to the quiescent emission. This area has a chromospheric tem-

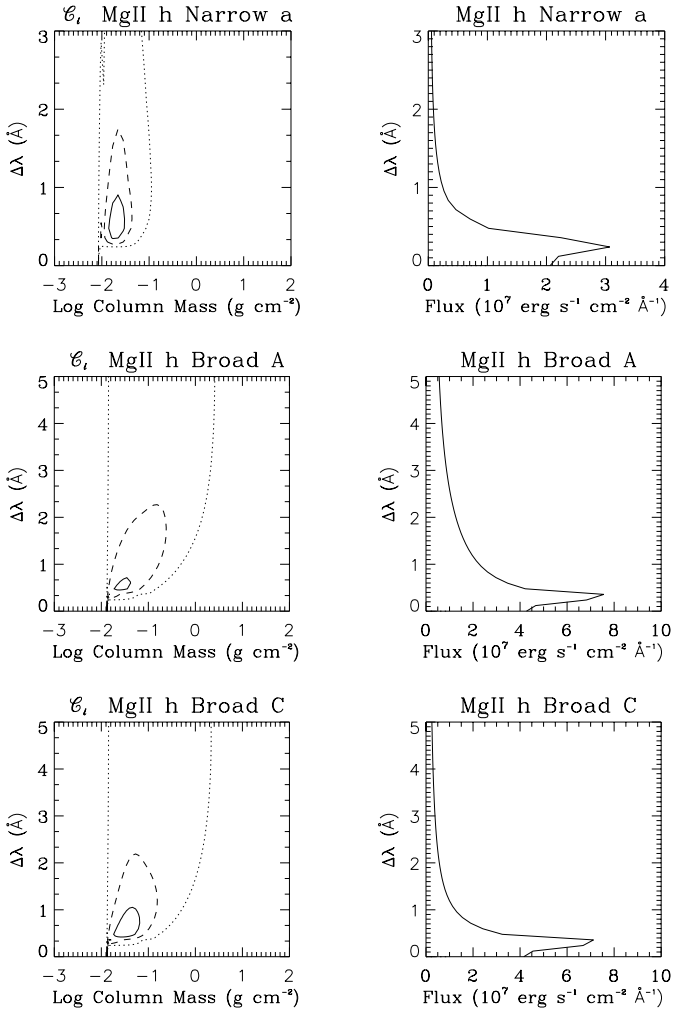

Fig. 12. Contribution function to the emergent radiation ($\mathcal{C}_l$)for the Mg II h line obtained from the narrow (a), broad (A), and broad (C) models (left panels) and emergent line flux (right panels). The maximum of the contribution function is set equal to one. The contour plot indicates the fractions 0.6 (solid), 0.2 (dashed) 0.05 (dotted).

perature ≈ 2000 K higher, a temperature minimum ≈ 1000 K higher, and a transition region pressure ≈ 60% higher than the rest of the stellar chromosphere. Our analysis gives very satisfactory fits of both the Mg II h and Hα lines and it is consistent with the stable photospheric spot configuration observed from 1981 to 1992 on V 711 Tau (Dorren & Guinan 1982, Rodonò et al. 1986, Vogt et al. 1999) and with photospheric Zeeman Doppler Imaging (Donati et al. 1990; 1992) which indicates the presence of a strong magnetic field at high latitudes on the K star covering about 18% of the stellar sufrace. Our results imply that the broad component derives from a higher level of chromospheric heating in such localised area and reinforces the idea that variability outside flares is mainly due to a gradual evolution of active regions.

Acknowledgements. Active star research at Catania Astrophysical Observatory and the Department of Physiscs and Astronomy of Catania University is funded by MURST (Ministero della Università e della Ricerca Scientifica e Tecnologica), and the Regione Siciliana, whose financial support is gratefully acknowledged.

References

Achmad L., De Jager C., Nieuwenhuijzen H., 1991, A&A 250, 445
Agrawal P.C., Vaidya J., 1988, MNRAS 235, 239
Busà I., Pagano I., Rodonò M., Neff J.E., Lanzafame A.C., 1999, A&A 350, 571
Byrne P.B., Abdul Aziz H., Amado P.J., et al., 1998, A&AS 127, 505
Carlsson M., 1986, Technical Report 33, Uppsala Astronomical Observatory
Cram L.E., Mullan D.J., 1979, ApJ 234, 579
Cram L.E., Giampapa M.S., 1987, ApJ 323, 316
Dempsey C.R., Neff J.E., Thorpe M.J., et al., 1996, ApJ 470, 1172
Donati J.F., Semel M., Rees D.E., Taylor K., Robinson R.D., 1990, A&A 232, L1
Donati J.F., Brown S.F., Semel M., et al., 1992, A&A 265, 682
Dorren J.D., Guinan E.F., 1982, ApJ 252, 296
Drake J., Brown A., Patterer R.J., et al., 1994, ApJ 421, L43
Fekel F.C., 1983, ApJ 268, 274
Frasca A., Catalano S., 1994, A&A 284, 883
Fontenla J.M., Avrett E.H., Loeser R., 1993, ApJ 406, 319
Griffiths N.W., Jordan C., 1998, ApJ 497, 883
Harper G.M., 1992, MNRAS 256, 37
Hauschildt P.H., Allard F., Baron E., 1999, ApJ 512, 377
Houdebine E.R., Panagi P., 1990, A&A 231, 459
Huang L., Zhai D., Catala C., Foing B.H., 1995, in: Huang L., Zhai D., (eds.) MUSICOS: Multi-Site Continuous Spectroscopy. Proc. of the 4th MUSICOS Workshop, p. 131
Jordan C., 1991, in: Ulmschneider P., Priest E.R, Rosner R., (eds.), Chromospheric and Coronal Heatings, p. 300
Kalkofen W., Ulmschneider P., Avrett E.H., 1999, ApJ 521, 141L
Lanzafame A.C., 1995, A&A 302, 839
Montes D., Fernandez-Figueroa M.J., De Castro E., Sanz-Forcada J., 1997, AAS 125, 263
Mauas P., Falchi A., Pasquini L., Pallavicini R., 1997, A&A 326, 249
Neff J.E., Pagano I., Rodonò M., 1995, in: Huang L., Zhai D. (eds.), MUSICOS: Multi-Site Continuous Spectroscopy. Proc. of the 4th MUSICOS Workshop, p. 157
Owen F. N., Jones T. W., Gibson D. M., 1976, ApJ 210, L27
Robinson R.D., Airapetian V.S., Maran S.P., Carpenter K.G., 1996, ApJ 469, 872
Rodonò M., Cutispoto G., Pazzani V. et al., 1986, A&A 165, 135
Rodonò M., Byrne P.B., Neff J.E. et al., 1987, A&A 176, 267
Strassmeier K.G., Hall D.S., Fekel F.C., Scheck M., 1993, A&A 100, 173
Trigilio C., Umana G., Migenes V., 1993, MNRAS 260, 903
Umana G., Trigilio C., Tumino M., Catalano S., Rodonò M., 1995, A&A 298, 143
Vernazza J.E., Avrett E.H., Loeser R., 1981, ApJS 45, 635
Vogt S.S., Penrod G.D., 1983, PASP 95, 565
Vogt S.S., Hatzes A.P., Micsh A.A., Kurster M., 1999, ApJS 121, 547
Wood B.E., Harper G.M., Linsky J.L., Dempsey C.R., 1996, ApJ 458, 761
Wood B.E., Linsky J.L., Ayres T.R. 1997, ApJ 478, 745